Electronic Supplementary Material (ESI) for Physical Chemistry Chemical Physics.
This journal is © the Owner Societies 2021

Electronic Supplementary Information

Tuning the Magnetic Properties of Diamagnetic Di-Blatter's Zwitterion to Antiferro- and Ferromagnetically Coupled Diradicals

Rishu Khurana,[†,‡] Ashima Bajaj,[†,‡] and Md. Ehesan Ali[*,†]

†*Institute of Nano Science and Technology, Sector-81, Mohali Punjab-140306, India*

‡*These authors contributed equally to this work.*

E-mail: ehesan.ali@inst.ac.in

Contents

1 Zwitterionic form of TPHA **S4**

2 Effect of length of coupler **S5**

2.1 Energetics comparison of different molecules S5

2.2 Energies of molecular orbitals of diradicals 5 and 6 . . . . . S6

2.3 Diradical character index (y) values S7

2.4 Occupation number of HONO and LUNO from CASSCF S8

2.5 Computation of Head-Gordon Index S8

2.6 Energies of frontier molecular orbitals S9

2.7 Computed exchange couplings using BS-DFT S9

2.8 Computed exchange couplings using BS(SF)-DFT S10

2.9 Computed exchange couplings using SF-TDDFT S10

2.10 Spin-decontaminated procedure in BS-DFT S10

2.11 Computed exchange couplings using CASSCF and NEVPT2 . . . . . S12

2.12 Calculations with larger coupler i.e., with n=7 to 9 . . . . . S13

2.13 $2J$ values with non-conjugated couplers S15

3 Substituent Effect **S16**

3.1 Hammett constants of different substituents S16

3.2 Interplanar angles S17

3.3 Effect of individual substitution of EDG and EWG S17

4 Diradicals with ferromagnetic coupling **S19**

4.1 BS-DFT computed exchange coupling S19

4.2 SF-TDDFT computed exchange coupling S20

4.3 Occupation number of HONO and LUNO from CASSCF S20

4.4 HOMA values S20

4.5 Energies of frontier orbitals S21

4.6 CASSCF and CASSCF-NEVPT2 computed exchange coupling S22

4.7 Aqueous pK_a value of corresponding phenols S22

1 Zwitterionic form of TPHA

The TPHA molecule adopts the zwitterionic configuration in its CSS state with the separation into 10π-anionic and 6π-cationic units. To elucidate this, different charge distribution schemes, including Löwdin, Mulliken and Hirshfeld charge distribution are used and are illustrated in Figure S1a, S1b and S1c and Table S1. Noteworthy, in this case, the positive and negative charges are not localized on the C1 and C4 only, but are delocalized over the 6π (blue part in Fig S1a) and 10π parts (red part in Fig S1a), therefore, we have taken the summation of the charges on all atoms in the two parts. The summed Löwdin charges on the negative part over all the atoms yield -0.36 a.u. charge. In contrast to this, the summed Löwdin charges on the positive part yield +0.36 a.u. Similarly, the summed Mulliken charges on the positive part is +0.51 a.u. and that on the negative part is -0.50 a.u. The corresponding Hirshfeld charges on the positive and negative parts are -0.42 and +0.41 respectively. Thus, all the considered charge distributions imply the formation of zwitterionic form in the CSS state. Moreover, in Figure S1d, the dipole moment of the molecule is plotted. Since, the dipole moment orients from positive to negative direction, it highlights the existence of positive and negative parts in the TPHA marking the zwitterionic state in the molecule. The electrostatic potential mapped on the electron density surface is also in favor of the zwitterionic ground state with separation of positive and negative parts (Figure S1e). Thus, TPHA adopts the zwitterionic ground state in its CSS state.

Table S1: Different charge distributions for the TPHA molecule.

Atom	**Löwdin**	**Mulliken**	**Hirshfeld**
C1	-0.12	-0.44	-0.09
C4	-0.09	-0.47	-0.07
Positive part	+0.36	+0.51	+0.41
Negative part	-0.36	-0.50	-0.42

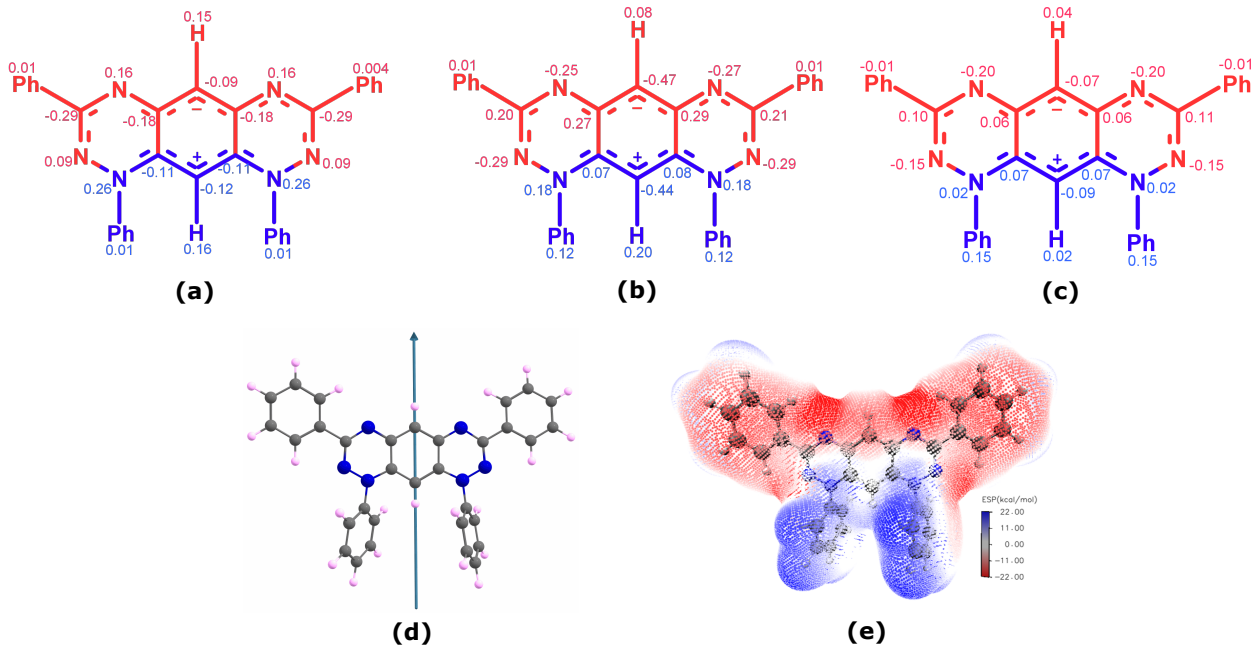

Figure S1: (a) The Löwdin charge density distribution (b) the Mulliken charge density distribution on different atoms of TPHA obtained at B3LYP/def2-TZVP level (c) Calculated dipole moment of TPHA with the direction of arrow from positive to negative part of the molecule (d) Electrostatic potential mapped on the electron density surface where red indicates negative charge and blue indicates positive charge.

2 Effect of length of coupler

2.1 Energetics comparison of different molecules

The molecules **1** to **6** are optimized in closed-shell singlet (CSS), open-shell singlet (OSS) and triplet (T) state. The optimized energies are collected in Table S2.

Table S2: DFT optimized energies (Eh) of molecules **1-6** in CSS, OSS and T states.

Molecules	Energies(Eh)		
	CSS	OSS	T
1	-1560.731910	-1560.731940	-1560.703722
2	-1714.320011	-1714.320450	-1714.306505
3	-1867.905945	-1867.909631	-1867.902685
4	-2021.491373	-2021.499045	-2021.495837
5	-2175.076950	-2175.085557	-2175.086306
6	-2328.664387	-2328.678135	-2328.680267

The relative energies of all the molecules referred to closed-shell state are given in Table S3.

Table S3: Relative energies referred to the CSS state for OSS and T states (in meV).

Molecules	**CSS** [E(CSS)-E(CSS)]	**OSS** [E(OSS)-E(CSS)]	**T** [E(T)-E(CSS)]
1	0.00	0.8	761.07
2	0.00	11.85	364.66
3	0.00	-99.52	88.1
4	0.00	-207.14	-120.52
5	0.00	-234.21	-254.59
6	0.00	-374.10	-432.12

From the relative energies, it is inferred that molecule **1** and **2** are stabilized in CSS state whereas molecule **3** and **4** are in OSS state. Molecules **5** and **6** possess triplet as ground state.

2.2 Energies of molecular orbitals of diradicals 5 and 6

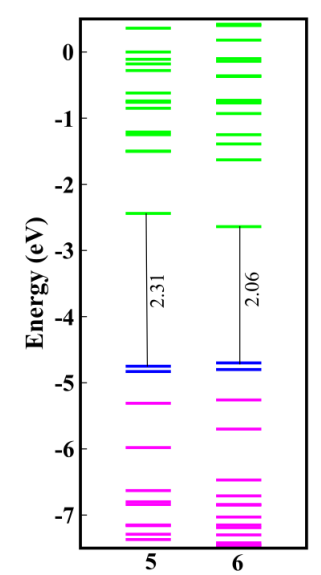

Figure S2: Molecular orbitals of α-spin electrons of molecules **5** and **6**. The pink, blue and green colours represent the doubly occupied, singly occupied and unoccupied orbitals respectively.

The spin-contamination for the diradicals **5** and **6** in the triplet state is up to 0.36. It is due to increased degeneracy of the molecular orbitals for these diradicals which can be observed from the Figure S2.

2.3 Diradical character index (y) values

To compute the diradical character as proposed by Yamaguchi et al.,[1] the occupation numbers of frontier natural orbitals have been taken. Since, there are large number of orbitals with partial occupation number, so instead of considering only the HOMO and LUMO, we have considered the occupation of larger number of orbitals. For molecule **1**, we have considered the occupation number of three occupied i.e. HOMO, HOMO-1 and HOMO-2 and three unoccupied i.e., LUMO, LUMO+1, LUMO+2, orbitals since, molecule **1** has benzene as coupler with 3π bonds. Further, proceeding towards molecule **2**, since there is addition of one benzene ring, which means addition of 2 π bonds, therefore, we have added two more occupied and unoccupied orbitals respectively. In a similar way, we have increased the two occupied and two unoccupied orbitals with addition of each benzene ring in moving from molecules from **3** to **6**. Taking the occupation numbers of these orbitals, T i.e., overlap integral is calculated and subsequently put in the equation for y to compute the diradical character index. The y values are collected in Table S4.

Table S4: Computed diradical character (y) for molecules **1-6**

Molecules	y **value**
1	0.28
2	0.53
3	0.65
4	0.75
5	0.78
6	0.80

2.4 Occupation number of HONO and LUNO from CASSCF

The orbital occupation number of HONO and LUNO obtained from CASSCF(10,10) are collected in Table S5. The occupation number of LUNO is subsequently increasing from 0.30 for molecule **1** to 0.95 for molecule **6** indicating increase in diradical character with larger number of benzene ring in the coupler.

Table S5: Occupation numbers of HONO (n_{HONO}) and LUNO (n_{LUNO}) obtained from CASSCF(10,10).

Molecules	n_{HONO}	n_{LUNO}
1	1.70	0.30
2	1.42	0.58
3	1.20	0.80
4	1.11	0.89
5	1.06	0.94
6	1.05	0.95

2.5 Computation of Head-Gordon Index

To compute the Head-Gordon Index for the molecules **1** to **6**, the occupation number of orbitals with partial occupancy are taken from CASSCF(10,10). The calculated values are tabulated in Table S6.

Table S6: Computed Head-Gordon index ($n_{u,nl}$) for the molecules **1-6**.

Molecules	$n_{u,nl}$
1	0.62
2	1.50
3	2.05
4	2.20
5	2.17
6	2.21

2.6 Energies of frontier molecular orbitals

Table S7: Energy difference between HOMO and LUMO (in eV) in closed shell singlet (CSS) and SOMO1 and SOMO2 (in eV) in triplet (T) states.

Molecules	**CSS**			**T**		
	E(H)	**E(L)**	Δ**E**$_{HL}$	**E(SOMO1)**	**E(SOMO2)**	Δ**E**$_{SS}$
1	-4.91	-2.51	2.40	-5.66	-3.87	1.79
2	-4.74	-3.00	1.74	-5.45	-4.23	1.22
3	-4.61	-3.36	1.25	-5.28	-4.50	0.78
4	-4.53	-3.59	0.94	-5.02	-4.65	0.37
5	-4.41	-3.77	0.64	-4.83	-4.75	0.08
6	-4.27	-3.88	0.39	-4.81	-4.70	0.11

2.7 Computed exchange couplings using BS-DFT

Table S8: Total energies and calculated exchange coupling constants for the diradicals using **BS-DFT; B3LYP/def2-TZVP** method.

Molecules	**Energy (Eh)**		$2J$**(cm**$^{-1}$**)**
	$<S^2>_{HS}$	$<S^2>_{BS}$	
3	-1867.902685	-1867.909005	-2774.64
	2.04	0.77	
4	-2021.495837	-2021.498662	-1240.04
	2.08	0.89	
5	-2175.086306	-2175.085557	328.84
	2.21	0.97	
6	-2328.680267	-2328.676170	1797.40
	2.36	1.03	

2.8 Computed exchange couplings using BS(SF)-DFT

Table S9: Total energies and calculated exchange coupling constants for the diradicals using **BS(SF)-DFT; B3LYP/def2-TZVP** method.

Molecules	**Energy (Eh)**		$2J$**(cm^{-1})**
	$<S^2>_{HS}$	$<S^2>_{BS}$	
3	-1867.902826	-1867.909145	-2773.82
	2.04	0.77	
4	-2021.496014	-2021.498838	-1239.46
	2.09	0.89	
5	-2021.498838	-2175.087628	306.32
	2.21	0.97	
6	-2328.680469	-2328.676379	1795.24
	2.36	1.04	

2.9 Computed exchange couplings using SF-TDDFT

Table S10: Total energies and calculated exchange coupling constants for the diradicals using **SF-TDDFT; BHHLYP/def2-TZVP** method.

Molecules	**Energy (eV)**		$2J$**(cm^{-1})**
	$<S^2>_{GS}$	$<S^2>_{ES}$	
3	0.544	0.747	-1632.05
	0.43	2.44	
4	0.725	0.789	-516.19
	0.79	2.58	
5	0.816	0.825	72.59
	2.76	1.23	
6	0.304	0.349	362.95
	2.03	1.42	

2.10 Spin-decontaminated procedure in BS-DFT

The Yamaguchi formalism leads to overestimated values when the spin polarization of the core becomes important. Therefore, it is required to extract the three main contributions to the magnetic exchange coupling i.e., a) direct exchange contribution, between the two unpaired electrons, b) kinetic exchange contribution, corresponding to relaxation of magnetic

orbitals in singlet state and c) spin polarization contribution, originating from different polarization of the electrons in the core orbitals in triplet and in singlet. The resultant of the three contributions provide the accurate magnitude of magnetic exchange coupling free from spin-contamination given by

$$J_{Tot} = J_o + \Delta J_{KE} + \Delta J_{CP} + \Delta J_{Other} \tag{1}$$

where J_o, ΔJ_{KE} and ΔJ_{CP} are the contributions from direct exchange, kinetic exchange and spin polarization of the core.

$$J_o = -\frac{E_{HS,RO} - E_{BS,RO}}{\langle S^2 \rangle_{HS,RO} - \langle S^2 \rangle_{BS,RO}} \tag{2}$$

$$\Delta J_{KE} = -\frac{E_{HS,RO} - E_{BS,UFC}}{\langle S^2 \rangle_{HS,RO} - \langle S^2 \rangle_{BS,UFC}} - J_o \tag{3}$$

$$\Delta J_{CP} = \frac{2(E_{BS,UFM} - E_{HS,UFM})}{2 - (\langle S^2 \rangle_{BS,UFC} + \langle S^2 \rangle_{BS,UFM})/2 + \langle S^2 \rangle_{BS,UFC}(\langle S^2 \rangle_{BS,UFM} - \langle S^2 \rangle_{BS,UFC})/2} - J_o - \Delta J_{KE} \tag{4}$$

$E_{HS,RO}$ is the energy obtained from the calculation performed in the HS state in Restricted Open-shell formalism. The spin-flip of one of the magnetic orbitals results in the energy of BS state in Restricted Open-shell formalism i.e. $E_{BS,RO}$. The relaxation of magnetic orbitals in the frozen core orbitals leads to $E_{BS,UFC}$ (UFC stands for Unrestricted with Frozen Core orbitals). The relaxation of core orbitals in (HS,RO) and (BS,RO) leads to $E_{HS,UFM}$ and $E_{BS,UFM}$ (UFM stands for Unrestricted with Frozen Magnetic orbitals).

Table S11: Computed Energies and <S^2> values of diradicals **3-6** obtained using LSCF method.

Molecules	**3**	**4**	**5**	**6**
E(HS,RO)	-1867.898256	-2021.490809	-2175.081286	-2328.659958
	2.00	2.00	2.00	2.00
E(HS,UFM)	-1867.902626	-2021.495750	-2175.087951	-2328.673931
	2.03	2.07	2.19	2.07
E(HS,U)	-1867.902683	-2021.495838	-2175.088171	-2328.680266
	2.04	2.09	2.21	2.36
E(BS,RO)	-1867.897860	-2021.490433	-2175.080655	-2328.652847
	1.00	1.00	1.00	1.00
E(BS,UFC)	-1867.904935	-2021.494454	-2175.082972	-2328.658858
	0.74	0.85	0.91	0.85
E(BS,UFM)	-1867.908868	-2021.498570	-2175.087423	-2328.670617
	0.77	0.88	0.95	1.03
E(BS,U)	-1867.909001	-2021.498655	-2175.087471	-2328.676178
	0.77	0.89	0.97	1.03

Table S12: Computed different contributions and total magnetic exchange coupling for molecules **3-6**.

Molecule	**3**	**4**	**5**	**6**
J_o	86.99	82.43	138.47	1560.71
$\Delta\ J_{KE}$	-1253.55	-778.63	-479.27	-1350.85
$\Delta\ J_{CP}$	73.16	156.34	447.64	430.07
J_{Other}	-22.43	-6.34	37.55	208.67
J_{Tot}	-1115.82	-546.19	144.40	848.59

2.11 Computed exchange couplings using CASSCF and NEVPT2

Table S13: Total energies and calculated exchange coupling constants for the diradicals using **CASSCF(10,10)** and **CAS(10,10)-NEVPT2** method.

Molecules	**CASSCF(10,10)**			**CAS(10,10)-NEVPT2**		
	E(HS)	**E(LS)**	$2J$**(cm^{-1})**	**E(HS)**	**E(LS)**	$2J$**(cm^{-1})**
3	-1857.220625	-1857.222139	-333.08	-1865.173269	-1865.180321	-1551.44
4	-2009.910567	-2009.910832	-58.30	-2018.540443	-2018.542475	-447.03
5	-2162.595917	-2162.595816	22.38	-2171.908049	-2171.907880	37.10
6	-2315.248468	-2315.244718	823.03	-2325.305596	-2325.301267	950.10

2.12 Calculations with larger coupler i.e., with n=7 to 9

We have performed additional calculations by increasing the length of coupler further from n=7 to 9. The computed exchange coupling along with the spin-squared values obtained from BS-DFT are tabulated in Table S14.

Table S14: Computed exchange coupling for diradicals **7-9** using BS-DFT.

Molecules	**Energy (Eh)**		$2J$(**cm**$^{-1}$)
	$<S^2>_{HS}$	$<S^2>_{BS}$	
7	-2482.270291	-2482.262953	3220.74
	2.55	1.11	
8	-2635.863408	-2635.853544	4329.26
	2.75	1.19	
9	-2789.456008	-2789.448677	3217.52
	2.97	1.63	

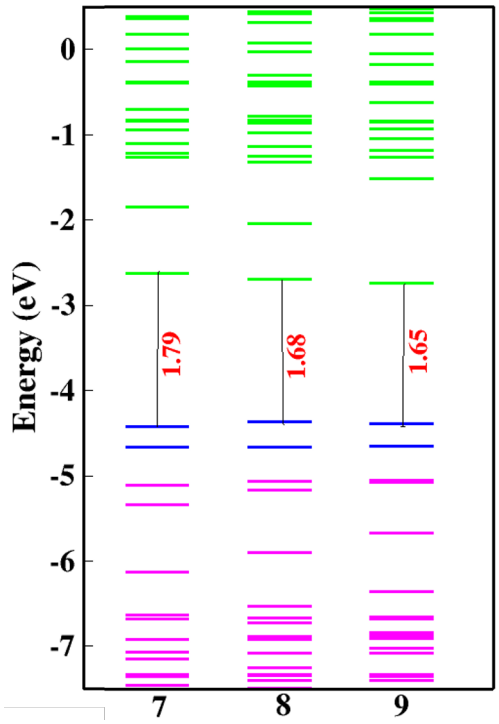

Figure S3: Molecular orbitals of α-spin electrons of molecules **7-9**.

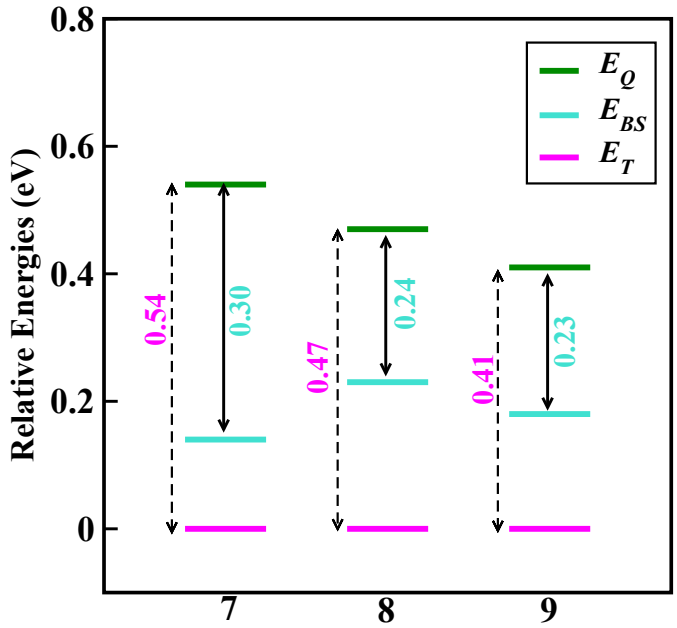

Figure S4: Relative energies of quintet and BS state relative to triplet state (which is the ground state) for molecules **7-9**.

The diradicals with larger coupler i.e., **7** to **9** possess high spin-contamination in HS as well as in BS state. The intrinsic open shell character, quasi-degenerate MOs (Figure S3) and the low-lying excited spin states (Figure S4) of polyacene coupler are the main reasons for the large spin-contamination in these molecules as also observed in our previous work.[2] Figure S4 reveals that upon increasing the length of coupler, the gap between quintet-triplet and quintet-BS state decreases, indicating that quintet state also starts playing an important role by mixing with triplet and BS state for higher polyacenes, which eventually results in high $<S^2>$ values in both triplet and BS state.

Table S15: Computed exchange coupling constants using CASSCF (10,10) and CAS(10,10)-NEVPT2.

Molecules	**CASSCF(10,10)**			**CAS(10,10)-NEVPT2**		
	E(HS)	**E(LS)**	$2J$**(cm^{-1})**	**E(HS)**	**E(LS)**	$2J$**(cm^{-1})**
7	-2467.889793	-2467.899268	-2079.27	-2478.731252	-2478.706427	5448.45
8	-2620.586709	-2620.594797	-1775.15	-2632.097779	-2632.060948	8083.47
9	-2773.269555	-2773.269306	-54.64	-2785.459174	-2785.451160	1758.86

The CASSCF(10,10) results in antiferromagnetic interactions for diradicals **7-9** in con-

trast to the ferromagnetic coupling predicted by DFT based methods. The reason for this inconsistency is the insufficient active space for the larger polyacene couplers with n=**7-9** which does not take into account all the orbitals originating from the center of the coupler. Interestingly, incorporating dynamical correlation with NEVPT2 yields balanced treatment of spin states with the correct prediction of ferromagnetic ground state, consistent with DFT based methods. The prediction of incorrect magnetic properties for the inorganic molecules by CASSCF is also witnessed by Singh et al. where they highlighted the importance of incorporating dynamical correlations to correctly produce the magnetic properties.[3]

2.13 2J values with non-conjugated couplers

Further, to validate that larger magnitude of 2J is due to polyacene coupler which possess inherent open-shell character, we coupled the two radical sites by hydrogenation of the coupler to make it non-conjugated (Figure S5) aliased as **3H-9H**. The 2J values obtained for these

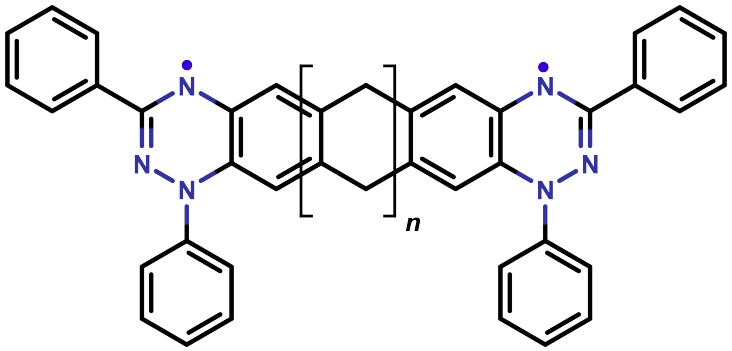

Figure S5: The Blatter's radicals coupled through non-conjugated coupler.

diradicals are collected in Table S16. The minuscule values obtained for diradicals with n>4 clearly reveals that the two radical centres behave as independent spin-centres with negligible exchange interactions existing between them. These couplers do not possess any inherent magnetic nature influencing exchange coupling between the radical centres. Moreover, the $<S^2>$ values in triplet and broken-symmetry states are 2.03 and 1.03 respectively, for all the diradicals (3H-9H) indicating is no spin contamination and that there are only two localized

spin centers in these diradicals.

Table S16: Computed magnetic exchange coupling constant for the diradicals with unconjugated spacers **3H-9H**.

Coupler	**2**J **(cm**$^{-1}$**)**	$<S^2>_{HS}$	$<S^2>_{BS}$	**Löwdin spin density**
3H	-21.84	2.03	1.03	0.66
4H	-25.32	2.03	1.03	0.66
5H	0.10	2.03	1.03	0.66
6H	0.06	2.03	1.03	0.66
7H	0.06	2.03	1.03	0.66
8H	0.28	2.03	1.03	0.66
9H	0.06	2.03	1.03	0.66

3 Substituent Effect

3.1 Hammett constants of different substituents

Table S17: Hammett constants $(\sigma_{para})^a$ of different substituents.

Substituents	σ_{para}
NMe_2	-0.83
NH_2	-0.66
OH	-0.37
NO_2	0.78
CN	0.66
CF_3	0.54

^{a} Taken from reference[4]

3.2 Interplanar angles

Table S18: Interplanar angles (ϕ_1 and ϕ_2) that EDG and EWG made with the benzene ring respectively in molecules **1a-i**.

Molecules	ϕ_1	ϕ_2
1a	121.46/121.59	121.18/120.58
1b	121.12/120.27	121.49/119.82
1c	120.50/120.95	120.06/120.09
1d	120.10/120.12	120.64/120.65
1e	120.04/120.06	121.15/120.90
1f	120.10/120.10	120.07/120.08
1g	120.77/118.78	120.66/120.68
1h	120.57/118.56	120.54/120.62
1i	120.67/118.70	120.11/119.81

3.3 Effect of individual substitution of EDG and EWG

To study the effect of individual substitution on the $<S^2>$ values and the energies of molecular orbitals, we have modeled molecules with individual substitution where either EDG or EWG is present and the other position is occupied by hydrogen atom (Figure S6. The computed $<S^2>$ values are collected in Table S19.

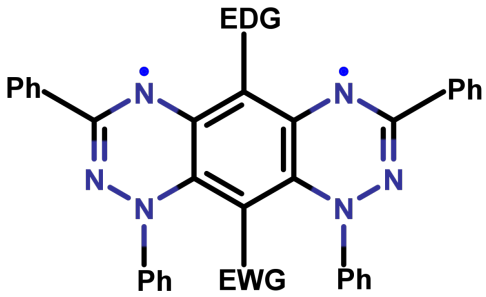

Molecule	EDG	EWG
1	H	H
1j	NMe_2	H
1k	NH_2	H
1l	OH	H
1m	H	CF_3
1n	H	CN
1o	H	NO_2

Figure S6: Modeled diradicals with individual substitution of different EDG and EWG on the parent TPHA aliased as **1j** to **1o**.

From the analysis of $<S^2>$ values in BS state, it is observed that the diradicaloid character is increased as compared to parent molecule TPHA. However, it is less than $<S^2>$ values of corresponding *push-pull* substitution.

Table S19: Computed $<S^2>$ values in HS and BS state at UB3LYP/def2-TZVP level.

Molecule	$<S^2>_{HS}$	$<S^2>_{BS}$
1	2.03	0.23
1j	2.04	0.51
1k	2.04	0.49
1l	2.04	0.40
1m	2.04	0.31
1n	2.04	0.17
1o	2.04	0.27

Further, the comparison of energies of HOMO and LUMO levels (Figure S7) reveal that when the EDG is attached, the energy of HOMO is elevated in comparison with that of parent molecule **1**. Moreover, the energy of LUMO is slightly elevated with respect to the LUMO energy level of **1**. In contrast to this, the EWG substitution results into the contrasting behavior where the energies of both HOMO and LUMO levels are lowered in comparison to the energies of TPHA. These observations are in line with the findings of Mao et al. where he proposed that EDG elevates the energies of HOMO/LUMO whereas EWG lowers them.[5]

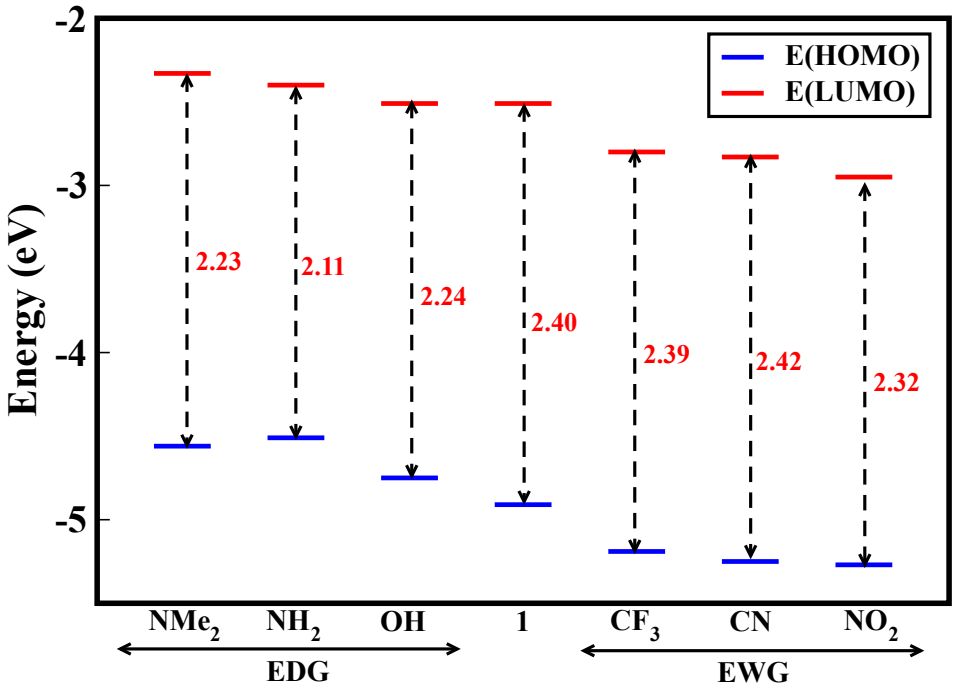

Figure S7: Energy difference (eV) between HOMO and LUMO in the structures optimized in open-shell singlet state for the molecules with individually substituted EDG and EWG.

4 Diradicals with ferromagnetic coupling

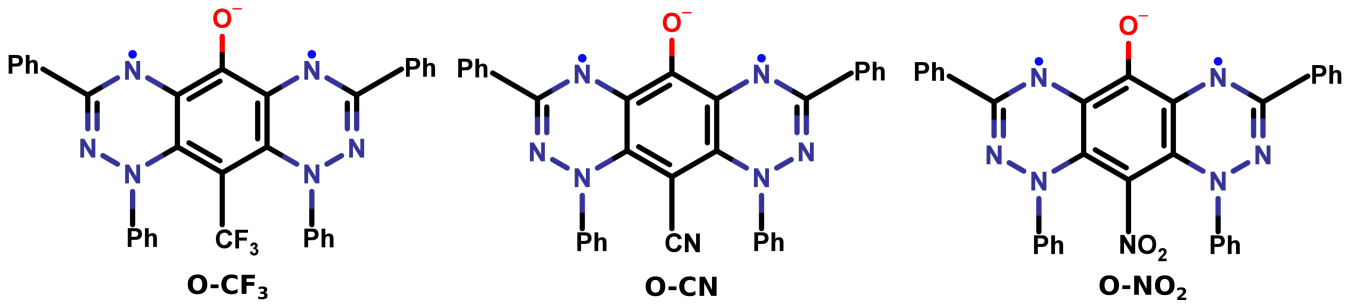

Figure S8: Diradicals obtained by substituting O^- as EDG and CF_3, CN and NO_2 as EWG.

4.1 BS-DFT computed exchange coupling

Table S20: Total energies and calculated exchange coupling constants for the three diradicals using **BS-DFT; B3LYP/def2-TZVP** method.

Diradical	**Energy (Eh)**		$2J$**(cm^{-1})**
	$<S^2>_{HS}$	$<S^2>_{BS}$	
O-CF_3	-1972.449082	-1972.449082	918.15
	2.03	0.97	
O-CN	-1727.627962	-1727.625439	1107.20
	2.03	0.99	
O-NO_2	-1839.892490	-1839.890909	693.58
	2.03	0.97	

4.2 SF-TDDFT computed exchange coupling

Table S21: Calculated exchange coupling constants for the three diradicals using **SF-TDDFT; BHHLYP/def2-TZVP** method.

Diradical	**Energy (eV)**		$2J$**(cm^{-1})**
	$<S^2>_{GS}$	$<S^2>_{ES}$	
O-CF_3	0.586	0.753	1352.50
	2.25	0.19	
O-CN	0.586	0.769	1471.35
	2.26	0.18	
O-NO_2	0.588	0.728	1130.20
	2.26	0.19	

4.3 Occupation number of HONO and LUNO from CASSCF

Table S22: Occupation number of HONO and LUNO from CASSCF(10,10) for the three diradicals.

Diradical	n_{HONO}	n_{LUNO}
O-CF_3	1.12	0.88
O-CN	1.13	0.87
O-NO_2	1.14	0.86

4.4 HOMA values

Table S23: Calculated HOMA values of the central benzene ring of the three diradicals.

Diradical	**HOMA**
O-CF_3	0.23
O-CN	0.20
O-NO_2	0.21

4.5 Energies of frontier orbitals

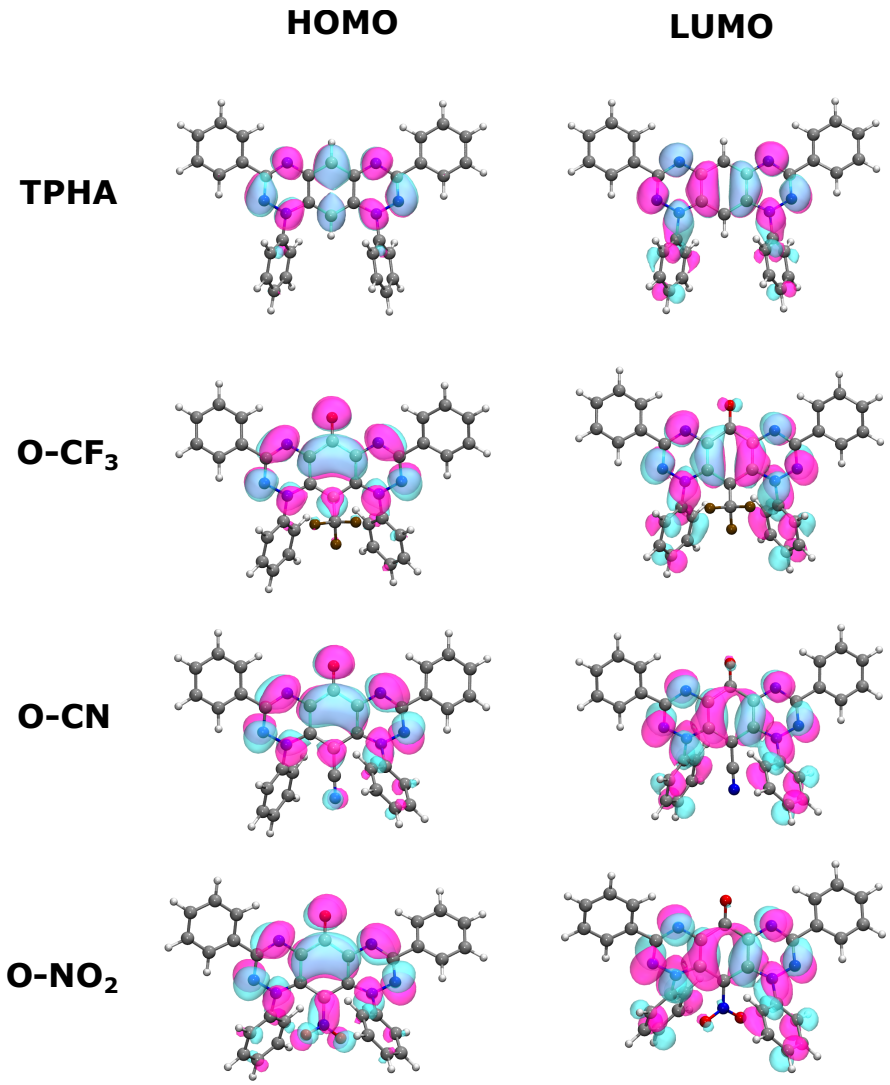

Figure S9: Frontier orbitals of TPHA and the three diradicals.

The analysis of frontier molecular orbitals reveal that their HOMO, in addition to the large coefficient at the centre of benzene ring, also exhibits large atomic coefficient at the EDG (O^-) and comparably small atomic coefficient at the EWG (CF_3, CN and NO_2), further elevating the energy of HOMO. Moreover, the LUMO also exhibits small atomic coefficient at the EDG (O^-), thereby, increasing the energy of LUMO in comparison to the parent molecule TPHA. Thus, the energies of both the HOMO and LUMO are increased but the

energy gap between the two orbitals will be decreased (∼1 eV) (Table S24) in comparison to TPHA (2.40 eV) leading to preferential strong diradical character in these molecules.

Table S24: Energy difference (ΔE_{HL}) between HOMO and LUMO (in eV) in closed shell singlet (CSS) state of the diradicals.

Molecules	**E(HOMO)**	**E(LUMO)**	ΔE_{HL}
TPHA	-4.91	-2.51	2.40
O-CF$_3$	-0.97	0.13	1.10
O-CN	-1.06	0.01	1.07
O-NO$_2$	-1.19	-0.13	1.03

4.6 CASSCF and CASSCF-NEVPT2 computed exchange coupling

Table S25: Total energies and calculated exchange coupling constants for the three diradicals using **CASSCF(10,10) and CASSCF(10,10)-NEVPT2** method.

Diradical	**CASSCF(10,10)**			**CAS(10,10)-NEVPT2**		
	E(HS)	**E(LS)**	$2J$**(cm^{-1})**	**E(HS)**	**E(LS)**	$2J$**(cm^{-1})**
O-CF$_3$	-1961.893180	-1961.882709	2298.11	-1969.779120	-1969.778378	162.85
O-CN	-1717.919742	-1717.911172	1880.89	-1725.183538	-1725.178368	1134.68
O-NO$_2$	-1829.695133	-1829.686775	1834.05	-1837.331006	-1837.326759	932.10

4.7 Aqueous pK$_a$ value of corresponding phenols

Further, to examine the formation of these diradicals from their corresponding phenols, we have calculated the aqueous pK$_a$ values of phenols The small pK$_a$ value of ∼3 (Table S26) is obtained for all the phenols, indicating that their proton is less tightly bind to them and can be easily removed. Thus, their conjugate bases (i.e., diradicals with O$^-$ EDG) can be readily formed. Further, the pK$_a$ value is directly related to Hammett constant where NO$_2$ substituted phenol has the smallest pK$_a$ value with large Hammett constant followed by CN and CF$_3$.

Table S26: The calculated aqueous pK_a values of the corresponding phenols of the three diradicals.

Molecule	**pK_a**
OH-CF_3	3.65
OH-CN	3.25
OH-NO_2	3.01

References

(1) Yamaguchi, K. The electronic structures of biradicals in the unrestricted Hartree-Fock approximation. *Chemical Physics Letters* **1975**, *33*, 330–335.

(2) Kaur, P.; Ali, M. E. First Principle Investigations of Long-range Magnetic Exchange Interactions via Polyacene Coupler. *Int. J. Quantum Chem.* **2021**, DOI: https://doi.org/10.1002/qua.26756.

(3) Singh, S. K.; Rajaraman, G. Deciphering the origin of giant magnetic anisotropy and fast quantum tunnelling in Rhenium (IV) single-molecule magnets. *Nat. Commun.* **2016**, *7*, 1–8.

(4) Hammett, L. P. The effect of structure upon the reactions of organic compounds. Benzene derivatives. *J. Am. Chem. Soc.* **1937**, *59*, 96–103.

(5) Mao, Y.; Head-Gordon, M.; Shao, Y. Unraveling substituent effects on frontier orbitals of conjugated molecules using an absolutely localized molecular orbital based analysis. *Chem. Sci.* **2018**, *9*, 8598–8607.